XANES Ti K-EDGE STUDY ON THE COORDINATION CHEMISTRY AND OXIDATION STATE OF Ti IN SYNTHETIC PYROXENE, OLIVINE, Fe-Ti OXIDES AND BASALTIC GLASSES UNDER LUNAR fO_2.

F.P. Leitzke[1], R.O.C. Fonseca[1], J. Göttlicher[2], R. Steininger[2], M. Lagos[1]; [1]Steinmann Institute, University of Bonn, Germany (felipe.leitzke@uni-bonn.de), [2]Institute for Photon Science and Synchrotron Radiation, ANKA, Karlsruhe Institute of Technology, Germany.

Introduction: Lunar petrogenesis has occurred under oxygen fugacity (fO_2) conditions below the Fe-FeO (Iron-Wüstite – IW) redox buffer [e.g., 1], which is ca. three orders of magnitude more reduced than the average value for the Earth's upper mantle [2]. Among the evidence found in lunar samples for such low redox conditions are the strong Eu anomaly in lunar basalts caused by fractionation of Eu^{2+} into the plagioclase [3,4], as well presence of metallic Fe, troilite (FeS), and armalcolite ($(Mg,Fe)Ti_2O_5$), the latter of which has long been known to potentially host reduced Ti^{3+} in its structure [5]. Lunar basalts are thought to result from partial melting of a mafic-ultramafic cumulate overturned mantle after the solidification of a magma ocean [6]. In addition, high-Ti mare basalts are considered to be produced under more reducing conditions than those prevalent throughout melting of low-Ti basalt sources (IW-2 and IW, respectively, see [7]). Even though the TiO_2-Ti_2O_3 redox buffer is located at more reduced conditions than IW, the idea that Ti^{3+} cannot coexist with high FeO contents have been refuted by direct measurements in refractory inclusions in meteorites, which yielded a $Ti^{3+}/\sum Ti$ ratio from 0.37 to 0.79 [8], as well as by the discovery of Tistarite (Ti_2O_3) in the Allende meteorite [9]. Regarding lunar magmatism, the dataset of studies dealing with X-ray absorption near edge structure (XANES) spectroscopy to determine redox transition of Ti is scarce, with recent works in lunar pyroxene and olivine from experiments and natural samples showing either significant [10, 11] or negligible [12] amounts of Ti^{3+}, depending on petrologic history, mineral and mantle source composition. Therefore, we present new Ti K-edge XANES spectroscopy measurements performed on a wide range of minerals (pyroxene, olivine, Fe-Ti oxides) and basaltic glasses under lunar conditions of fO_2, which can be used to better constrain the $Ti^{3+}/\sum Ti$ of the lunar mantle.

Experimental and Analytical Techniques: Experiments were conducted in 1 bar vertical tube gas-mixing furnaces through the loop technique, using either Pt or Re wire, for Fe-poor and Fe-rich compositions respectively. Temperature ranged between 1100 and 1300 °C and fO_2 between IW-1.5 and IW-1.8, imposed through a CO-CO_2 atmosphere. Run products were analyzed for major elements (CaO, MgO, Al_2O_3, SiO_2, Cr_2O_3, TiO_2, and FeO) using a JEOL JXA 8900 electron microprobe in WDS (Wavelength Dispersive) mode, with accelerating voltage at 15 kV, 15 nA beam current and an electron beam defocused to 5 µm. Ti K-edge XANES spectra were acquired using a Si (111) double crystal monochromator at the SUL-X beamline of the ANKA synchrotron facility (Karlsruhe, Germany). The X-ray beam was focused to 50 µm at sample position with a KB mirror system on each phase. Measurements had to be performed in fluorescence mode due to the thickness of the polished sections. To reduce self-absorption effects which occur at high Ti concentrations in fluorescence mode, the sample surface was aligned 85 ° towards the beam (close to perpendicular position) and the sample surface – detector angle resulted then in 5 ° (close to grazing exit conditions). Sample chamber was kept under vacuum in order to avoid absorption of the low energy X-rays under air. Energy shifts were monitored by measuring Ti metal foil between every five points and aligned to 4966 eV (first maximum of the first derivative). Because crystal orientation can be a source of uncertainty [9], we have measured several points randomly allocated among the crystals in different experiments at the same fO_2. To determine Ti coordination and oxidation of state in the experiments, the 1s-3d energy shifts were used, following [9,13,14], and the lever rule between standards representative of each one of the end-members. XANES data were processed with the Athena programme of the IFEFFIT software package [15].

Results: Typical run products had large (> 100 µm) euhedral to subhedral crystals (diopside, augite, enstatite, forsterite, armalcolite and ilmenite) in chemical equilibrium with quenched silicate glass (Figure 1).

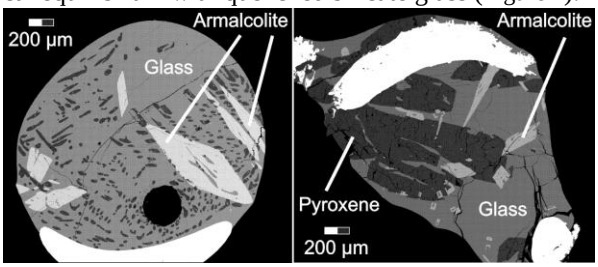

Figure 1 – Back-scattered electron images of typical experimental run products at one-atmosphere gas mixing furnaces.

Crystal size was controlled by the cooling ramp and the TiO_2 content of the silicate melt, which proved to have a depolymerizing effect [16]. Among the silicates, diopside and augite crystals had the largest $TiO_{2(t)}$ contents ranging from 0.49 to 2.89 wt. % and 0.01 to 0.09 atoms per formula unit (apfu), which is not high enough for accurately determining $Ti^{3+}/\sum Ti$ using the

electron microprobe [9]. The ^{IV}Al of cpx did not exceed 0.10 apfu. Enstatite and Forsterite had a maximum Ti content of 1.43 wt. % (0.04 apfu) and 0.13 wt. %, respectively. Armalcolite crystals ranged from Fe- to Mg-rich and $Ti^{3+}/\sum Ti$ calculated using microprobe data is ca. 0.1-0.2, the same as observed for ilmenite. Ti K-edge XANES spectra show a clear shift in energy for the absorption edge features from oxidizing to reducing conditions [9,13], for example, about 3 eV from TiO_2 to Ti_2O_3 at the main-edge feature (Figure 2).

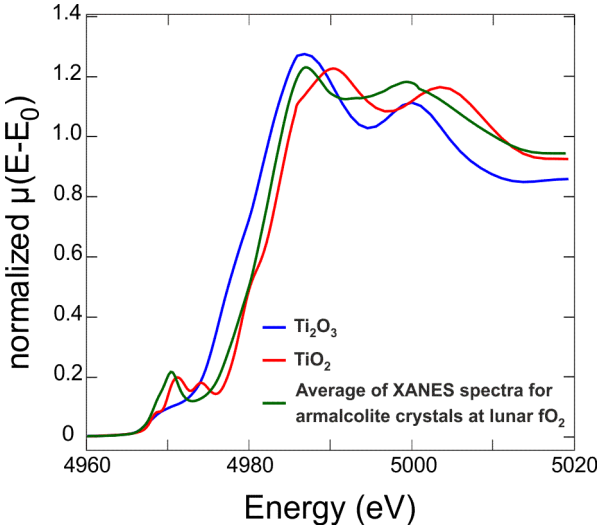

Figure 2 –XANES spectra of two reference materials and the average of all armalcolite crystals equilibrated below IW.

Preliminary XANES data yield an average valence for Ti of 3.6, i.e., a $Ti^{3+}/\sum Ti$ value of 0.4 for crystalline phases with a lower limit of 0.1 and an upper limit of 0.7 (Figure 3). Silicate glasses show that Ti is mainly tetravalent, which indicates that a redox exchange occurred in the glass during the experiments, quenching or after samples were mounted (Figure 3). Pre-edge features also show that the coordination number of Ti varies from average V-fold in the silicate glass, which is in agreement to the expected for basaltic glasses [17], to VI-fold in the Fe-Ti oxides and a mixture between VI and IV-fold coordination in the pyroxenes. The maximum amount of Ti in tetrahedral coordination in the pyroxenes in our study is ca. 40 %.

Discussion: Studies of direct measurement in pyroxene and olivine from natural lunar samples originated under reducing conditions have reported $Ti^{3+}/\sum Ti$ average values of 0.1-0.2 [11] or 0.3-0.4 [18] for primitive lunar magmas, which would become more oxidized as fractional crystallization continues, and Ti^{3+} is retained at the source due to its higher crystal/silicate melt compatibility. Some of these values are lower than the average reported here, which can be explained by the fact that in our experiments the Ti^{3+} content of the crystals is solely a function of the fO_2 imposed by the experimental atmosphere. When compared to experimental results on equivalent compositions, our data for pyroxene are in good agreement to [10], who reported Ti valence of ca. 3.5 for pyroxenes equilibrated at ΔIW -2. Previous microprobe detections of Ti^{3+} for lunar Fe-Ti oxides [e.g., 5,19] pointed to a $Ti^{3+}/\sum Ti$ ratio of 0.1-0.2, which is within error of the ones obtained by our X-ray absorption spectroscopic measurements. When recalculated to $TiO_{2(t)}$, our estimates of ca. 30-40 % Ti_2O_3 can be used to correct the excess of TiO_2 measured by EMP-WDS. Future work on the substitution mechanisms of Ti^{3+} in the crystals and combining XANES data on experiments and natural samples will provide new insights into lunar magmatism and the fO_2 evolution of the solar system.

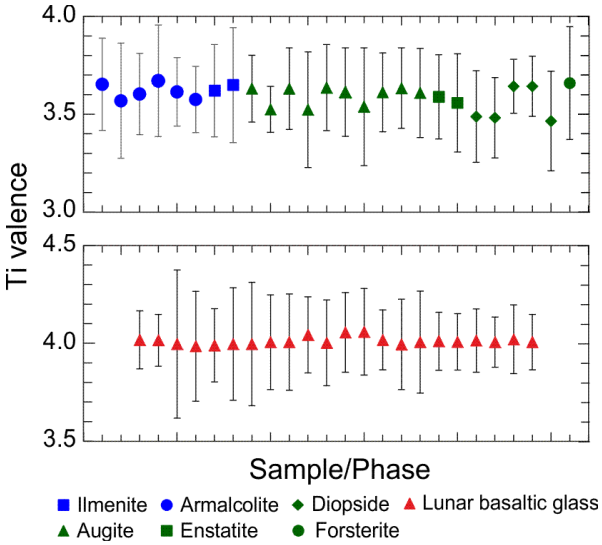

Figure 3 – Summary of Ti valence state for crystals and silicate glasses equilibrated between ΔIW -1.5 to -1.8.

References: [1] Papike J. J. et al. (2005) *Am Mineral., 90,* 277-290. [2] Ballhaus C. (1993) *CMP, 114,* 331-348. [3] Brophy J. G. and Basu A. (1990) *LPSC XX,* 25-30. [4] O'Hara M. J. and Niu Y. (2015) *GSA Spec. Paper, 514,* 339-366. [5] Stanin F. T. and Taylor L. (1980) *LPSC XI,* 117-124. [6] Ringwood A. E. and Kesson S. E. (1976) *LPSC VII,* 1697-1722. [7] Fonseca R. O. C et al. (2014) *EPSL, 404,* 1-13. [8] Ma C. and Rossmann G.R. (2009) *Am Mineral, 94,* 841-844. [9] Simon S. B. et al. (2007) *GCA, 71,* 3098-3118. [10] Krawczynski M. J. et al. (2010) *LPSC XLI,* #1825. [11] Simon S. B. et al. (2016) *LPSC XLVII,* #1251. [12] Simon S. B. et al. (2014) *LPSC XLV,* #1063. [13] Waychunas G. (1987) *Am Mineral., 72,* 89-101. [14] Farges F. et al. (1995) *GCA, 60,* 3023-3038. [15] Ravel B. and Newville M. (2005) *JSR, 12,* 537-541. [16] Leitzke et al. (2016) *Chem. Geol., 440,* 219-238. [17] Farges F. and Brown Jr. G.E. (1997) *GCA, 61,* 1863-1870. [18] Sung, C. et al. (1974) *LPSC V,* 717-726. [19] Pavicevic et al. (1972) *LPSC III,* 295-303.